JACS
JOURNAL OF THE AMERICAN CHEMICAL SOCIETY

ARTICLE

pubs.acs.org/JACS

# Membrane-Mediated Induction and Sorting of K-Ras Microdomain Signaling Platforms

Katrin Weise,[†] Shobhna Kapoor,[†] Christian Denter,[†] Jörg Nikolaus,[‡] Norbert Opitz,[§] Sebastian Koch,[⊥,#] Gemma Triola,[⊥,#] Andreas Herrmann,[‡] Herbert Waldmann,[⊥,#] and Roland Winter*[,†]

[†]Physical Chemistry I, Biophysical Chemistry, Faculty of Chemistry, TU Dortmund University, Otto-Hahn-Strasse 6, D-44227 Dortmund, Germany

[‡]Institute of Biology/Biophysics, Humboldt University Berlin, Invalidenstrasse 42, D-10115 Berlin, Germany

[§]Max Planck Institute of Molecular Physiology, Otto-Hahn-Strasse 11, D-44227 Dortmund, Germany

[⊥]Chemical Biology, Max Planck Institute of Molecular Physiology, Otto-Hahn-Strasse 11, D-44227 Dortmund

[#]Faculty of Chemistry, TU Dortmund University, Otto-Hahn-Strasse 6, D-44227 Dortmund, Germany

Supporting Information

**ABSTRACT:** The K-Ras4B GTPase is a major oncoprotein whose signaling activity depends on its correct localization to negatively charged subcellular membranes and nanoclustering in membrane microdomains. Selective localization and clustering are mediated by the polybasic farnesylated C-terminus of K-Ras4B, but the mechanisms and molecular determinants involved are largely unknown. In a combined chemical biological and biophysical approach we investigated the partitioning of semisynthetic fully functional lipidated K-Ras4B proteins into heterogeneous anionic model membranes and membranes composed of viral lipid extracts. Independent of GDP/GTP-loading, K-Ras4B is preferentially localized in liquid-disordered ($l_d$) lipid domains and forms new protein-containing fluid domains that are recruiting multivalent acidic lipids by an effective, electrostatic lipid sorting mechanism. In addition, GDP-GTP exchange and, thereby, Ras activation results in a higher concentration of activated K-Ras4B in the nanoscale signaling platforms. Conversely, palmitoylated and farnesylated N-Ras proteins partition into the $l_d$ phase and concentrate at the $l_d/l_o$ phase boundary of heterogeneous membranes. Next to the lipid anchor system, the results reveal an involvement of the G-domain in the membrane interaction process by determining minor but yet significant structural reorientations of the GDP/GTP-K-Ras4B proteins at lipid interfaces. A molecular mechanism for isoform-specific Ras signaling from separate membrane microdomains is postulated from the results of this study.

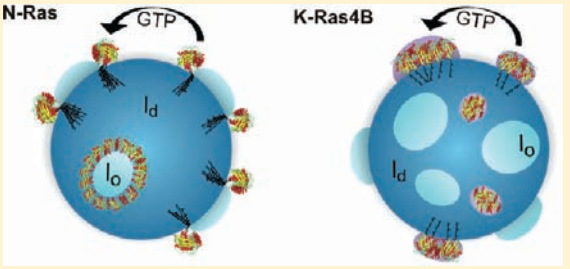


## INTRODUCTION

Ras proteins are small GTPases that act as molecular switches between a GDP-bound inactive and a GTP-bound active state.[1−3] Constitutively activated K-Ras4B contributes to the initiation and maintenance of many tumor cell types, including those of the pancreas, colon, and lung.[4] A prerequisite for the regulation of signal transmission from cell surface receptors to intracellular signaling cascades—including the oncogenic potential of Ras proteins—is the anchorage of Ras in the cytosolic leaflet of cellular membranes.[5−7] The cytosolic face of the plasma membrane, endosomes, and lysosomes of mammalian cells is enriched in acidic phospholipids, such as phosphatidylserine (PS) as well as phosphatidylinositol (PI) and polyphosphoinositides (PPI), due to an asymmetric distribution of neutral and anionic phospholipids in the two bilayer leaflets of membranes.[8,9]

The highly conserved N-terminal G-domain of Ras encompasses all interaction sites for activators and effectors. Conversely, the plasma membrane localization of Ras has been determined to be directed by the Ras isoform specific, post-translationally modified C-terminal sequence[6,7,10] that constitutes together with the linker domain the hypervariable region (HVR). For the 4B splice variant of K-Ras (K-Ras4B), this membrane interacting and targeting signal consists of a C-terminal polybasic stretch of six contiguous lysines in a total of eight that immediately precedes the terminal farnesylated and carboxymethylated cysteine residue (Figure 1).[2,7,11]

Two models have been proposed for the selective targeting of K-Ras4B to the cytosolic face of the plasma membrane: One involves a nonspecific electrostatic interaction of the lipidated polybasic domain with anionic phospholipids in the plasma membrane,[7,9,12,13] the other involves binding of K-Ras4B to a specific membrane-bound protein receptor.[14] Furthermore, a possible involvement of microtubules in the directing process has

**Received:** August 20, 2010
**Published:** December 9, 2010





dx.doi.org/10.1021/ja107532q | J. Am. Chem. Soc. 2011, 133, 880–887

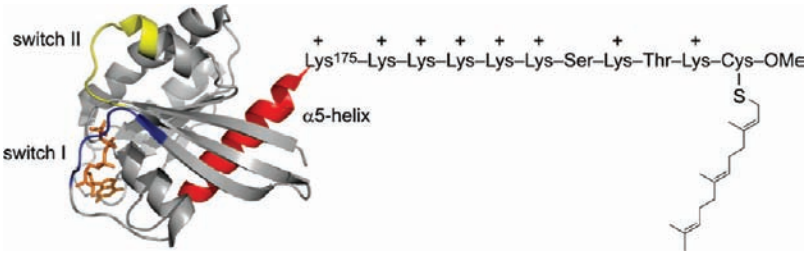


**Figure 1.** Schematic representation of the semisynthetic K-Ras4B protein. The synthesized, lipidated K-Ras4B peptide was ligated to a truncated K-Ras4B protein expressed in *E.coli* to yield the *S*-farnesylated K-Ras4B protein bearing an additional cysteine between $Gly^{174}$ and $Lys^{175}$. The structure of the G-domain was adopted from the pdb (3GFT) to highlight the switch I region (residues 32−38; blue), switch II region (59−67; yellow), and α5-helix (151−166; red). For the fluorescence experiments, the protein core is labeled with BODIPY.

been suggested.[15] It has also been shown recently that K-Ras4B can be redirected from one target membrane to another depending on the surface charge density of the membrane and the net charge of the protein.[8] Accordingly, an increase in cytosolic calcium will result in a decrease of the most-negative plasma membrane's surface charge, rendering it comparable to the intermediate negative charge density of endomembranes, which now compete effectively for binding of K-Ras4B.[8] On the other hand, a reduction of the positive net charge of the polybasic domain by phosphorylation of serine 181 within the HVR of K-Ras4B leads to an association not only with the plasma membrane, but also to a substantial degree with endocytic membranes.[9,16,17] Hence, the intracellular transport of K-Ras4B between subcellular compartments may be driven by electrostatic interactions, with the polybasic domain acting as a probe for the electronegative surface potential of the membrane.[18,19]

Recent experimental work indicates that signaling of K-Ras4B is restricted to particular plasma membrane microdomains in detecting a clustering of GTP- and GDP-loaded K-Ras4B into cholesterol-independent and actin-dependent but spatially distinct nanodomains.[20−22] This K-Ras4B nanocluster assembly is thought to lead to the formation of a local environment highly enriched in acidic phospholipids, thus enabling a localized high-affinity binding domain for effector proteins. However, the mechanism underlying K-Ras4B nanoclustering is currently unknown. To yield a pictorial view of the localization process of K-Ras4B in heterogeneous membranes up to a single molecule level, high-resolution imaging using confocal laser scanning and tapping-mode atomic force microscopy has been used in the present study. Semisynthetic fully functional lipidated, GDP-loaded and GTP-loaded (GppNHp-bound state as a nonhydrolyzable GTP analog) K-Ras4B proteins were synthesized,[23] and their partitioning into a newly designed, heterogeneous anionic model membrane system as well as a membrane system that mimics the lipid composition of biological membranes was investigated. The results lead to the postulation of a molecular mechanism for isoform-specific Ras signaling from separate membrane microdomains. Furthermore, time-dependent FTIR experiments reveal changes in G-domain orientation and strength of membrane interaction upon GDP-GTP exchange and thereby Ras activation.

## RESULTS

**Establishment of a Heterogeneous Anionic Model Membrane System.** Up to now, ternary lipid mixtures such as DOPC/DPPC/Chol have been widely used in studies of the interaction of lipidated proteins, such as N-Ras, with zwitterionic model raft membranes.[24] Since it is known that the positively charged lysines in the K-Ras4B membrane anchor region can strongly interact with negatively charged lipids, a heterogeneous anionic model membrane system needed to be established. Previous reports revealed no specific binding of the polybasic K-Ras4B domain to any of the common mono- and polyanionic phospholipids of the inner plasma membrane.[19] Here we used phosphatidylglycerol (PG) as an established model for anionic phospholipids. Calorimetry, FTIR spectroscopy, confocal fluorescence microscopy, and AFM data revealed that incorporation of 10 to 20 mol % PG (corresponding to a DOPC/DOPG/DPPC/DPPG/Chol lipid bilayer with a molar ratio of 20:5:45:5:25 and 15:10:40:10:25, respectively) still leads to segregation of the lipid mixture into liquid-ordered ($l_o$) and liquid-disordered ($l_d$) domains at room temperature (data not shown). The corresponding AFM analysis shows one homogeneous lipid bilayer on mica with isolated islands of fluid ($l_d$) domains in a coherent pool of raft-like ($l_o$) protruding phase (Supporting Information, Figure S1).[23]

**Interaction of K-Ras4B with GUVs Containing Charged Domains.** In a first set of experiments, the partitioning of GDP- and GTP-loaded, farnesylated and BODIPY-labeled K-Ras4B into GUVs composed of DOPC/DOPG/DPPC/DPPG/Chol 15:10:40:10:25 was analyzed by confocal fluorescence microscopy at room temperature. In confocal fluorescence microscopy, phases can be identified as ordered or fluidlike disordered on the basis of the known partitioning behavior of appropriate fluorescence probes, such as *N*-Rh-DHPE. Figure 2 shows the GUV images taken after the binding process of K-Ras4B to the lipid vesicles was completed ($t \approx 2$ h). Panels a and c exhibit the round-shaped domains typical for coexisting liquid-like phases.[25,26] The bright red areas with embedded, homogeneously distributed *N*-Rh-DHPE correspond to $l_d$ domains, whereas the dark domains consist mainly of $l_o$ phase. By simultaneous inspection of the rhodamine (red) and BODIPY (green) channel, where the latter identifies the localization of the BODIPY-labeled protein within the lipid assembly (panels b and d), one can directly follow the incorporation of the protein into the lipid microdomains. Superposition of both channels clearly shows that both GDP- and GTP-loaded K-Ras4B are essentially localized in the $l_d$ phase of the lipid bilayer system (the respective images coincide in both cases). Quantification of the protein partitioning can be estimated by determining the background-corrected fluorescence intensity ratio of $l_o$ versus $l_d$ phases (cf. Materials and Methods). An average fluorescence intensity ratio of $0.18 \pm 0.05$ and $0.11 \pm 0.03$ has been determined for the inactive and active K-Ras4B, respectively, thus confirming the preferred $l_d$ phase partitioning

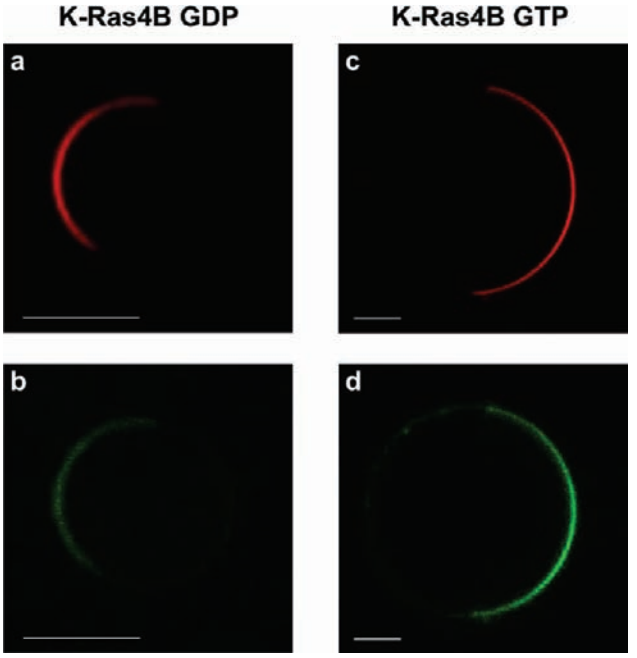


**Figure 2.** Confocal laser scanning microscopy images of the partitioning of K-Ras4B GDP (a,b) and K-Ras4B GTP (c,d) into GUVs. GUVs were composed of DOPC/DOPG/DPPC/DPPG/Chol 15:10:40:10:25, that segregate into $l_o$ and $l_d$ domains at room temperature. *N*-Rh-DHPE was used as membrane marker, labeling preferentially the $l_d$ domains (red channel, a and c); the K-Ras4B proteins were BODIPY-labeled (green channel, b and d). The overlay of the red and green channel shows that both K-Ras4B GDP and K-Ras4B GTP insert preferentially into the $l_d$ lipid phase, which is confirmed by the determined fluorescence intensity ratio of 0.20 for image b and 0.14 for image d, respectively. The scale bar represents 10 $\mu$m.

of both K-Ras4B proteins in showing values (82 to 89%) similar to those of $l_d$ phase fluorescent markers.

**AFM Study of K-Ras4B Interaction with Phase-Separated Anionic Membranes.** To yield complementary structural data on a smaller, nanometer length scale, the interaction of the GDP- and GTP-loaded, farnesylated K-Ras4B with lipid domains of the negatively charged heterogeneous membrane was followed by AFM. A sample consisting of one lipid bilayer with coexisting $l_o$ and $l_d$ domains on mica was examined at the beginning of each time-lapse tapping-mode AFM experiment (Figure 3, a and d). Using the technique of direct injection of a solution containing K-Ras4B protein into the AFM fluid cell, the same region of the lipid bilayer can be observed before and after incorporation of the protein.

The incubation of the lipid bilayer with both active and inactive K-Ras4B did not influence the lateral membrane organization initially, i.e., coexisting $l_d$ and $l_o$ domains of similar shape and size can still be distinguished, and the height difference between both phases remains ~1.0 nm (Figure 4). The data also show that the inactive and active K-Ras4B are readily incorporated (on a minute time scale) and exclusively located in the bulk $l_d$ phase upon binding to the lipid bilayer (Figure 3 panels b and e, respectively). A quantitative AFM analysis reveals a mean height of 2.0 ± 0.7 nm (mean value ± s.d., $n$ = 304) for K-Ras4B GDP, and a similar value of 2.5 ± 0.4 nm ($n$ = 296) was determined for the GTP-loaded K-Ras4B (Figure 4). These dimensions correspond roughly to the diameter of a Ras molecule.[27] Whereas N-Ras proteins bearing at least one farnesyl anchor showed a

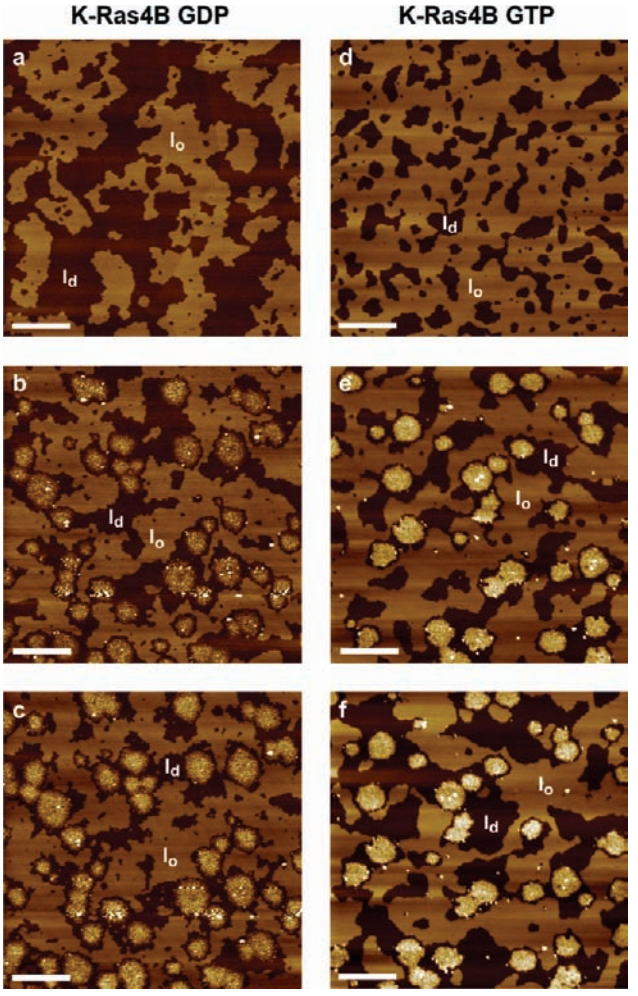


**Figure 3.** AFM images of the time-dependent partitioning of GDP- and GTP-loaded K-Ras4B into lipid bilayers consisting of DOPC/DOPG/DPPC/DPPG/Chol 20:5:45:5:25. The AFM images are shown before (a and d) and at selected time points ($t \approx 6$ and 5 h, b and e, respectively; $t \approx 24$ h, c; and $t \approx 20.5$ h, f) after injection of 200 $\mu$L of K-Ras4B in 20 mM Tris, 7 mM $MgCl_2$, pH 7.4 ($c_{K\text{-}Ras4B}$ = 2 $\mu$M) into the AFM fluid cell. The overall height of the vertical color scale from dark brown to white corresponds to 6 nm for all images. The scale bar represents 2 $\mu$m.

time dependent diffusion into and subsequent clustering in the $l_o/l_d$ phase boundary region,[24,28] formation of new domains with accumulated protein inside a fluidlike environment was observed for both K-Ras4B proteins after membrane insertion (Figures 3 and 4). These new domains with enriched GDP- and GTP-loaded K-Ras4B exhibit an average lateral dimension of ~1.5 $\mu$m or less and show a thickness which is 0.9 ± 0.1 nm ($n$ = 119) and 1.8 ± 0.2 nm ($n$ = 89) larger than that of the purely fluid lipid phase for the GDP and GTP bound state, respectively. Both the lateral dimensions of the protein clusters and the domain thicknesses critically depend on the protein concentration and preexisting lateral organization of the membrane. Whereas the lateral dimensions of the protein domains enriched in GDP- and GTP-loaded K-Ras4B are similar, the protein clusters of active and inactive K-Ras4B can be clearly distinguished by the different domain thicknesses in all cases. This indicates that the clustering effect is even more pronounced for the active K-Ras4B since the thicker domains argue for a stronger enrichment in protein (Figure 4). The increased domain thickness can be

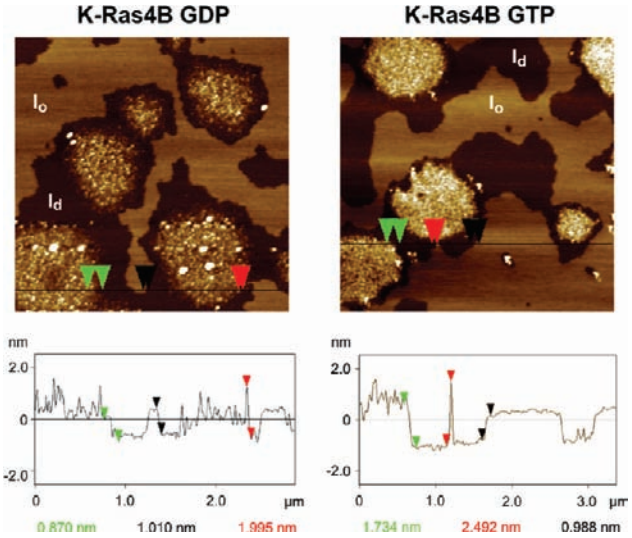


**Figure 4.** Analysis of the AFM images of GDP- and GTP-loaded K-Ras4B. Zoom of the lower and middle left area of the AFM images at $t \approx 6$ and 5 h (panels b and e, respectively, in Figure 3) and analysis of the corresponding AFM images for K-Ras4B GDP (left) and K-Ras4B GTP (right) ($c_{K\text{-}Ras4B}$ = 2 $\mu$M). In the upper part, the section profiles of the AFM images are shown with a vertical color scale from dark brown to white corresponding to an overall height of 5 nm. The horizontal black line is the localization of the section analysis given at the bottom, indicating the vertical distances between pairs of arrows (black, $l_o/l_d$ phase difference; green, thickness difference of the new domains enriched in K-Ras4B compared to $l_d$ domains; and red, size of the K-Ras4B proteins).

explained by a tighter packing of the Ras molecules via a different orientation of the protein with respect to the membrane interface. Interestingly, these newly formed domains are stable over the whole time range covered, whereas the lipids in the bulk $l_d$ phase still exhibit a high lateral mobility (Figure 3, panels c and f).

**Structural Aspects of the K-Ras4B Membrane Interaction.** To reveal possible changes in the structure of K-Ras4B during the membrane interaction process, time-dependent FTIR spectroscopic measurements have been carried out. Structural changes of K-Ras4B in the presence of large unilamellar vesicles (LUVs) composed of DOPC/DOPG/DPPC/DPPG/Chol 20:5:45:5:25 were followed as a function of time at 25 °C, with spectra collected every 10 min. The individual secondary structural elements contributing to the amide-I′ band have been determined by using the local minima of the concomitant second derivative spectra and the local maxima of its Fourier self-deconvolution (FSD; Figure 5 and Supporting Information, Figure S2). Figure 5 shows the FSD of the time evolution of the normalized FTIR spectra of the amide-I′ band (a and c) and the concomitant second derivative spectra (b and d) for the GDP- and GTP-loaded K-Ras4B, respectively. At the beginning of the membrane interaction process ($t$ = 1.5 min), subbands at about 1673, 1661, 1648, and 1637 $cm^{-1}$ and a shoulder at 1626 $cm^{-1}$ can be detected for the inactive K-Ras4B GDP. With time, a shift to lower wavenumbers was observed for the overall spectra that is accompanied by a small change in spectral shape (panel a), suggesting some minor but significant reorientational changes upon membrane binding. The analysis of the second derivative spectra (panel b) revealed a decrease in the band intensity at 1661 $cm^{-1}$ with time, which is accompanied by a concomitant increase in the band intensity at 1654/1656 $cm^{-1}$ that is indicative for α-helical structures. The comparison with an equivalent measurement of K-Ras4B GDP in bulk solution (20 mM Tris, 7 mM $MgCl_2$, pD 7.4; Supporting Information, Figure S3), that is, in the absence of membrane, that exhibits a corresponding subband for α-helical structures at about 1658 $cm^{-1}$, indicates a marked interaction of the respective α-helical region of the protein with the lipid bilayer interface (shift to lower wavenumbers). Furthermore, a gradual shift to 1671 $cm^{-1}$ was detected with time for the subband at 1673 $cm^{-1}$ that is attributed to turns and loops, which again would argue for a stronger interaction of these structure elements with the membrane.[29] The analysis of the amide-I′ band of K-Ras4B GDP in bulk solution yields a secondary structure content of 24% α-helix, 39% $\beta$-sheet, 15% turns and loops, and 21% random coil, in reasonable agreement with literature data (Supporting Information, Figure S3).[30] Minor differences may be due to different transition dipole moments of the various conformers and the absence of the HVR in the NMR and X-ray data. The corresponding fits of the time-dependent FTIR spectra of Ras residing in the membrane revealed, as expected, no significant changes in secondary structure of K-Ras4B GDP within the experimental error over the whole time range covered (Supporting Information, Figure S2c); that is, the structure of K-Ras4B GDP is not drastically affected by the membrane interaction, only minor reorientational changes seem to occur upon membrane binding.

The same holds true for the active, GTP-loaded K-Ras4B. Similar to the K-Ras4B GDP behavior, a shift of the overall spectra to lower wavenumbers was observed with time, which is accompanied by small changes in spectral shape (Figure 5c), pointing toward minor but significant structural reorientations of the protein upon membrane insertion. Subbands at about 1672, 1662, 1651, and 1637 $cm^{-1}$ and a shoulder at 1626 $cm^{-1}$ can be detected for K-Ras4B GTP at the beginning of the membrane interaction process ($t$ = 1.5 min), that stay constant over the whole time range covered (panel d). However, the intensity of the band at 1672 $cm^{-1}$ decreases with time, which is accompanied by a corresponding increase at 1662 $cm^{-1}$. Similar to the results for the inactive K-Ras4B, no marked changes in secondary structure could be detected within the experimental error by the fits of the time-dependent FTIR spectra for K-Ras4B GTP (Supporting Information, Figure S2f), again suggesting minor orientational rearrangements, only. The absence of the shift of the α-helical subband at 1662 $cm^{-1}$ upon membrane binding might imply a higher reorientational flexibility of the helices of K-Ras4B GTP as compared to K-Ras4B GDP, and hence reveals minor intermolecular interactions of the K-Ras4B in its membrane-bound form upon nucleotide exchange.

Orientational changes of the protein can also be revealed by following the insertion of K-Ras4B into lipid monolayers composed of DOPC/DOPG/DPPC/DPPG/Chol with infrared reflection absorption (IRRA) spectroscopy. Corresponding IRRA spectra of the amide-I′ region of K-Ras4B GDP reveal a band maximum within 1643−1641 $cm^{-1}$ over the whole time course of the membrane interaction process, indicating a rather stable and relatively fixed orientation of the protein at the lipid interface during protein adsorption (Supporting Information, Figure S4a). In contrast, a gradual shift in wavenumber from 1638 to 1647 $cm^{-1}$ could be observed for K-Ras4B GTP with time (Figure S4c), suggesting a reorientation of the active protein at the lipid interface during membrane insertion. When compared with simulations of the IRRA spectra performed for the Ras G-domain,[31] it can be concluded that K-Ras4B GTP achieves on

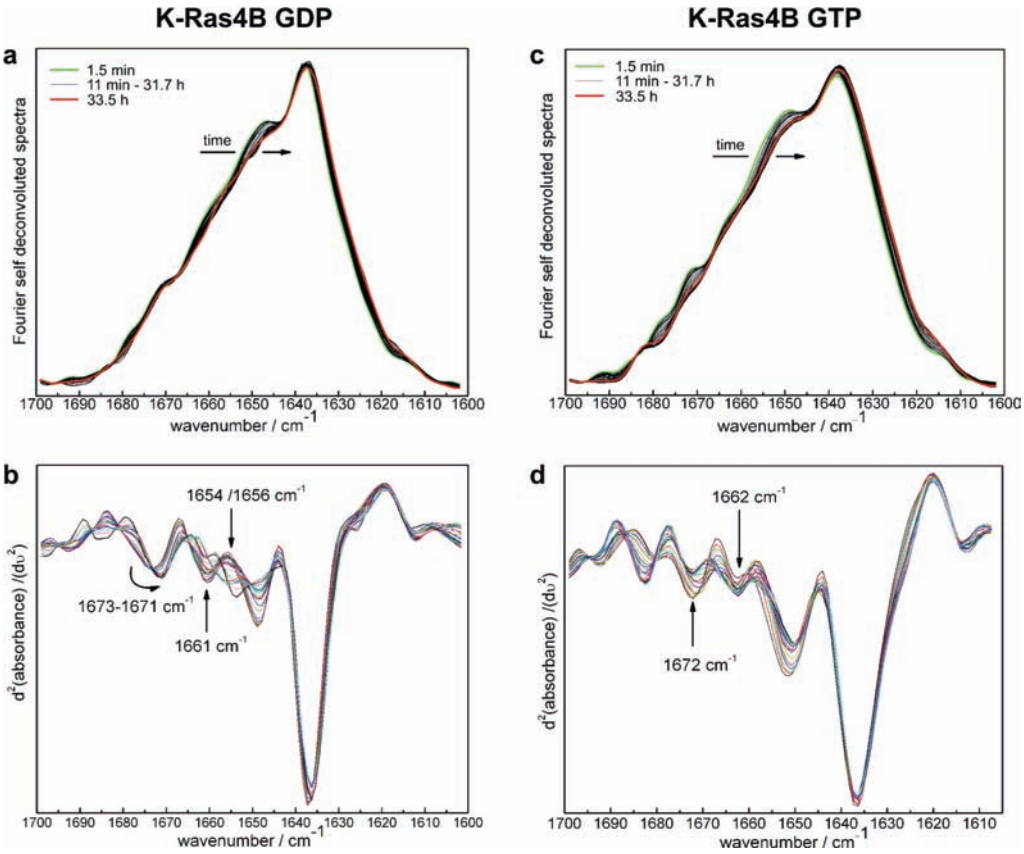


**Figure 5.** FTIR spectroscopic analysis of the GDP- and GTP-loaded K-Ras4B membrane interaction. Panels a and c show the normalized FSD FTIR spectra for the time evolution of the amide-I′ band of K-Ras4B GDP (a) and K-Ras4B GTP (c) in the presence of DOPC/DOPG/DPPC/DPPG/Chol 20:5:45:5:25 at 25 °C. The corresponding second derivative spectra are given in panels b and d. Arrows indicate the spectral shifts (in b) as well as the increasing (b, at 1654/1656 $cm^{-1}$; d, at 1662 $cm^{-1}$) and decreasing (b, at 1661 $cm^{-1}$; d, at 1672 $cm^{-1}$) intensities as a function of time.

average an orientation that is compatible with an essentially random orientation with respect to the lipid interface, suggesting a higher reorientational flexibility for the active K-Ras protein, which would be in agreement with the transmission FTIR experiments. In IRRAS, generally the combined effects of a change in orientation along with a change in secondary structure (including changes in the strength of interaction) are detected. Since there are no secondary structural changes for the protein in the presence of the membrane (as evident from the transmission FTIR experiments), the shift observed for K-Ras4B GTP in the IRRA spectra can be assigned to a reorientation of the protein at the membrane interface. Moreover, the amide-I′ band for the inactive K-Ras4B appears at lower wavenumbers compared with K-Ras4B GTP at saturation pressures (Figure S4), suggesting a different orientation and stronger interaction with the membrane interface.

**Interaction of K-Ras4B with Membranes Composed of Viral Lipid Extracts.** To evaluate the biological relevance of the membrane partitioning process observed in the heterogeneous anionic model membrane system, corresponding studies with lipid bilayers made from the envelope membrane of influenza viruses (strain A/Japan/305/57) have been carried out. As influenza virus is assembled at and is budding from the plasma membrane of host cells, the envelope mimics essentially the lipid composition of the plasma membranes with some preference for raft lipids.[32] Confocal fluorescence microscopy experiments of GUVs made of this biological mixture indicated the coexistence of raft-like $l_o$ and fluid $l_d$ domains, with R18 used as a fluorescent marker for the $l_d$ phase. Figure 6 shows that both active and inactive K-Ras4B are mainly localized in the fluid $l_d$ domains of the viral membrane. Quantification of the protein partitioning yielded average fluorescence intensity ratios of 0.39 ± 0.12 and 0.34 ± 0.13 for the inactive and active K-Ras4B, respectively. Since R18 showed a mean fluorescence intensity ratio of 0.18 ± 0.09 (i.e., 82% $l_d$), phase partitioning of both K-Ras4B proteins can be essentially assigned to the fluid $l_d$ phase (≥61%). Whereas for N-Ras a significant incorporation of the protein in the $l_o/l_d$ phase boundaries of the viral membrane was revealed by fluorescence intensity profiles,[28] no such effect could be detected for K-Ras4B even after incubation times up to 48 h (cf. Figure 7).

## DISCUSSION AND CONCLUSIONS

The Ras oncoproteins most frequently found in human tumors are activated K-Ras and N-Ras. Hence, the Ras isoform specific differences in signaling and lateral segregation to specific nanoscale compartments on the plasma membrane are issues under high scrutiny in the fields of biochemistry and biophysics. In a recent comparable approach, we were already able to demonstrate that palmitoylated and farnesylated N-Ras undergoes a time-dependent diffusion and subsequent clustering in the $l_o/l_d$ phase boundary region of the heterogeneous model and viral membranes, independent of GDP/GTP-loading (cf. Figure 7).[24,28,33] A monofarnesylated N-Ras that resembles the depalmitoylated

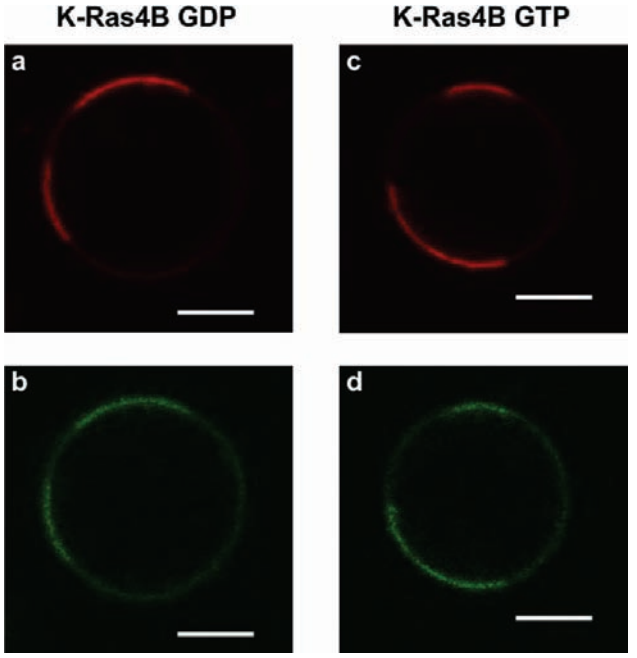


**Figure 6.** Confocal laser scanning microscopy images (equatorial plane, $t \approx 12$ h) of the partitioning of K-Ras4B GDP (a, b) and K-Ras4B GTP (c, d) into GUVs from viral membranes. GUVs were prepared from lipid extracts of influenza virus (strain A/Japan/305/57) and incubated with BODIPY-labeled K-Ras4B protein for up to 48 h at 20 °C. Both BODIPY-labeled K-Ras4B proteins (green channel, b and d) are colocalized with R18 (red channel, a and c) that is enriched in fluid $l_d$ phase, indicating a preferential partitioning of K-Ras4B into $l_d$ domains of influenza virus lipid-derived membranes. The determined fluorescence intensity ratios are 0.13 (R18), 0.30 (K-Ras4B GDP), 0.09 (R18), and 0.28 (K-Ras4B GTP) for images a, b, c, and d, respectively. The scale bar represents 5 $\mu$m.

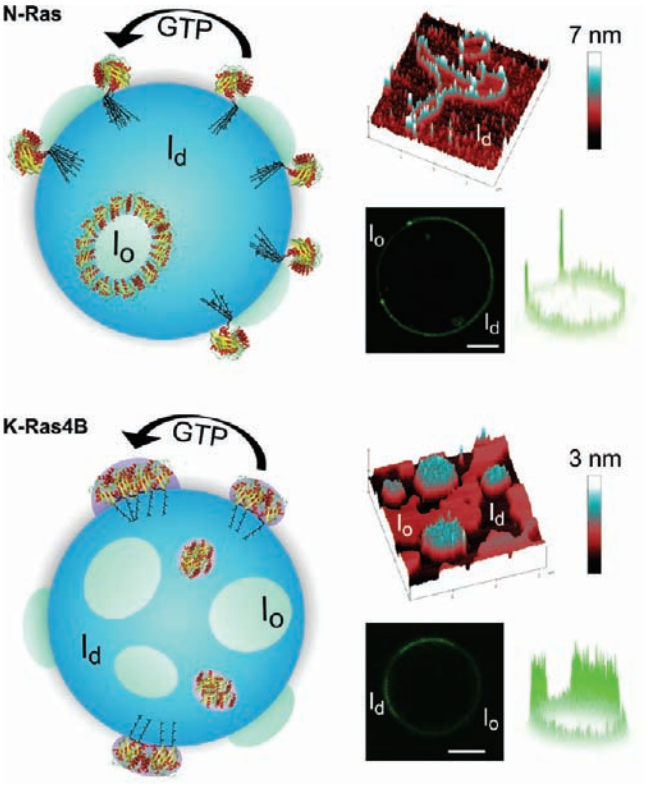


**Figure 7.** Schematic model for N- and K-Ras4B localization in vesicular heterogeneous model biomembranes with liquid-disordered ($l_d$) and liquid-ordered ($l_o$) domains (left). Please note that the schematic view is not to scale. Whereas N-Ras partitions into the fluid-like phase of the membrane and subsequently diffuses to the $l_d/l_o$ phase boundaries of the subcompartments as visualized by fluorescence microscopy and AFM (top right, with the clustered proteins depicted in blue-white in the 3D AFM images), K-Ras4B forms new protein-enriched fluid domains within the bulk fluid phase upon membrane binding and is thought to recruit multivalent anionic lipids by an effective, electrostatic lipid sorting mechanism (bottom). The GDP to GTP nucleotide exchange leads to changes in G-domain orientation and a stronger enrichment in protein in the signaling platform.

form of the natural N-Ras in the course of the acylation/deacylation cycle[10,34−36] also partitions into the $l_d$ phase and concentrates in the $l_o/l_d$ domain interface.[24] Similar mechanistic studies on the lateral segregation of signaling proteins bearing a farnesyl anchor and a polybasic amino acid stretch, such as K-Ras4B, were missing until now. In contrast to N-Ras, spontaneous formation of new domains with accumulated protein residing within the bulk fluid phase of an anionic model raft membrane has been observed for GDP- and GTP-loaded K-Ras4B in the present study. Thereby, the bulky and branched farnesyl anchor prevents partitioning of K-Ras4B into highly ordered raft-like domains and accommodates more easily into disordered lipid domains. Such sorting effect has also been observed for other bulky and branched lipid anchors such as the tocopherol moiety.[37] A similar membrane partitioning behavior of K-Ras4B as in anionic model membranes was also observed in influenza virus lipid-derived membranes mimicking the composition of mammalian plasma membranes.

To further address the question whether the sorting of K-Ras4B is solely goverend by electrostatic interactions with the anionic lipids in the membrane, the partitioning of K-Ras4B was also studied in zwitterionic heterogeneous membranes (DOPC/DPPC/Chol 25:50:25). Rather unexpectedly, a similar membrane partitioning behavior was detected in neutral and negatively charged membranes for both, active and inactive K-Ras4B, with even similar dimensions for the protein enriched domains (Supporting Information, Figures S5 and S6). Hence, electrostatic interactions between the polybasic domain of K-Ras4B and anionic lipids do not seem to be essential for the formation of new protein enriched domains in the fluid phase of the membrane. However, this sorting effect of K-Ras4B is nevertheless controlled by electrostatic interactions between the positively charged lysines and the negatively charged phosphate of the lipid head groups since the monofarnesylated and noncharged N-Ras revealed a clustering at the lipid domain boundaries under similar conditions.[24] It has in fact been observed that the polybasic stretch of K-Ras4B is able to induce a local positive electrostatic potential that attracts multivalent acidic lipids.[38] Such scenario would also be in agreement with a model proposed by McLaughlin and co-workers that suggested sequestration of polyvalent ($PIP_2$ and $PIP_3$) but not monovalent acidic lipids via nonspecific interactions for membrane-bound basic peptides.[38,39] Recent reports also demonstrate the requirement of highly charged polyphosphoinositides for the membrane interaction of K-Ras4B *in vivo*.[40]

Overall, these results provide a molecular mechanism for isoform-specific Ras signaling from separate membrane microdomains (Figure 7). For N-Ras, the expulsion of the protein to the interfacial region combined with a minimization of the line

energy between neighboring domains is likely to be one of the key parameters controlling the size and dynamic properties of its signaling platform (Figure 7, top). Conversely, for K-Ras4B, electrostatic interactions seem to control the membrane interaction process. As a consequence, polyvalent acidic lipids can be recruited by an effective lipid sorting mechanism and new fluid domains with higher anionic charge density and incorporated K-Ras4B protein are formed (Figure 7, bottom). In fact, the free energy of binding increases by about 1 kcal/mol per Lys under physiological conditions.[41] These results are in accord with *in vivo* studies that proposed the existence of K-Ras4B nanoclusters with higher contents of acidic phospholipids.[20−22]

For both, N-Ras and K-Ras4B no drastic influence of GTP/GDP-loading on the membrane interaction process could be observed. Both membrane arrested states lead to nanoscale signaling platforms. However, the tendency toward clustering seems to be more pronounced for the active (GTP-bound) states of the proteins (Figure 7). Moreover, as visible in the AFM images, domains seem to largely sort by size. Interestingly, recent experimental and theoretical works have shown that partial budded membrane domains repel due to membrane mediated interactions which can be explained by an interplay between line tension and bending rigidity effects.[42] The spontaneous Ras isoform-specific sorting and the collective lateral organization of induced membrane domains could potentially operate as an effective, high fidelity signaling platform with distinct signal outputs for the Ras isoforms. In fact, nanoclustering has been proposed in *in vivo* experiments to be critical for signal transmission, as it allows the cell to respond to low signal inputs with a fixed output.[43]

Next to the lipid anchor system, the G-domain provides additional determinants for K-Ras4B membrane interactions. Upon membrane binding of the inactive K-Ras4B, a shift of the α-helical subband to lower wavenumbers was observed in the FTIR spectra that is indicative for stronger membrane interactions. Since the α5-helix directly precedes the HVR (Figure 1), this effect can be attributed to an exposure of the α5-helix in the G-domain to the lipid interface. GDP-GTP exchange and thereby K-Ras4B activation leads to structural reorientations mainly in the switch I and switch II regions of the G-domain,[44] which is likely to reduce the α5-helix−membrane interactions observed in the FTIR data. The weaker interaction and higher reorientational flexibility of active K-Ras4B at the membrane interface were further confirmed by corresponding IRRAS experiments. In fact, it appears from recent molecular dynamics (MD) simulations that the HVR is the stabilizing motif for K-Ras4B membrane interaction and that the process involves mainly the C-terminal part of the HVR for K-Ras4B GTP, but the whole HVR for K-Ras4B GDP.[45] The α5-helix is closer to the membrane interface in the inactive state, which enables stronger membrane interaction. Hence, the FTIR and IRRA spectroscopy results support recent insights from MD simulations in showing minor but yet significant structural reorientations of the GDP/GTP-K-Ras4B proteins at lipid interfaces. However, the effect of the α5-helix−membrane interaction needs to be studied in more detail, for example, by specific protein mutations, in future work.

## ■ MATERIALS AND METHODS

**Materials and Sample Preparation.** The phospholipids 1,2-dioleoyl-*sn*-glycero-3-phosphocholine (DOPC), 1,2-dioleoyl-*sn*-glycero-3-phospho-(1′-*rac*-glycerol) sodium salt (DOPG), 1,2-dipalmitoyl-*sn*-glycero-3-phospho-(1′-*rac*-glycerol) sodium salt (DPPG), and 1,2-dipalmitoyl-*sn*-glycero-3-phosphocholine (DPPC) were purchased from Avanti Polar Lipids (Alabaster, AL). Cholesterol (Chol) was from Sigma-Aldrich and the fluorescent lipids *N*-(lissamine rhodamine B sulfonyl)-1,2-dihexadecanoyl-*sn*-glycero-3-phosphoethanolamine triethylammonium salt (*N*-Rh-DHPE), 4,4-difluoro-5,7-dimethyl-4-bora-3a,4a-diaza-*s*-indacene-3-propionic acid, succinimidyl ester (BODIPY FL, SE), and octadecylrhodamine B chloride (R18) from Molecular Probes (Invitrogen). Details on the preparation of lipid films are given in the Supporting Information.

**Protein Synthesis.** The synthesis of the K-Ras4B proteins is described in detail in ref 23. Briefly, the *S*-farnesylated K-Ras4B protein was synthesized by a combination of expressed protein ligation (EPL) and lipopeptide synthesis. Details on the nucleotide exchange and BODIPY-labeling of K-Ras4B proteins are available in the Supporting Information.

**Atomic Force Microscopy (AFM).** The preparation of the supported lipid bilayers and the AFM setup is described in detail in ref 24 and the Supporting Information. For the protein−membrane interaction studies, 200 μL of K-Ras4B protein in 20 mM Tris, 7 mM $MgCl_2$, pH 7.4 ($c_{protein}$ = 2 μM) were injected into the AFM fluid cell at room temperature and allowed to incubate for 1 h. Measurements were performed on a MultiMode scanning probe microscope with a NanoScope IIIa controller (Digital Instruments, Santa Barbara, CA) and usage of a J-Scanner (scan size 125 μm). Images were obtained by applying the tapping mode in liquid with oxide-sharpened silicon nitride (DNP-S) or sharp nitride lever (SNL) probes mounted in a fluid cell (MTFML, Veeco, Mannheim, Germany).

**Confocal Laser Scanning Microscopy of Model Membranes.** GUVs were prepared by electroformation[32,46,47] in a temperature controlled homemade chamber on optically transparent and electrically conductive indium tin oxide (ITO) coated glass slides (SPI Supplies, West Chester, USA). The BODIPY-labeled K-Ras4B proteins were added via an injection-channel ($c_{K\text{-}Ras4B}$ = 0.1−0.2 μM), yielding a final BODIPY concentration in the cell-chamber of 10 nM and a final molar ratio of lipid/*N*-Rh-DHPE of 500:1. Images were recorded with a confocal laser scanning microscope (Biorad MRC 1024, extended for multiphoton excitation, now Zeiss, Germany) coupled via a side-port to an inverted microscope (Nikon, Eclipse TE-300 DV, infinity corrected optics) enabling fluorescence excitation in the focal plane of an objective lens (Nikon Plan Fluor 40×, NA = 0.6, and Nikon Plan Appochromat VC 60× A WI, NA = 1.2 collar rim corr.). Details of the experimental setup are provided in the Supporting Information. Quantification of the protein partitioning was carried out by determining the background (BG) corrected fluorescence intensity ratios (FIR) of $l_o$ versus $l_d$ phases within the different phase regions of interest, that is, FIR = $[I(l_o) - I(BG)]/[I(l_d) - I(BG)]$ and calculating the average value for at least eight GUVs. The analysis was performed similar to that described in ref 48.

**Confocal Laser Scanning Microscopy of Viral Membranes.** GUVs were prepared by electroformation[46] on titan plates from viral lipids, isolated from influenza virus A/Japan/305/57 according to Bligh and Dyer.[49] A final BODIPY concentration of 1.7 and 2.3 μM R18 was used in a μ-Slide VI chamber (ibidi, Martinsried, Germany). Confocal images of the equatorial plane of the GUVs in 250 mM glucose, 5.8 mM $NaH_2PO_4$, 5.8 mM $Na_2HPO_4$, pH 7.2 were taken using an inverted confocal laser scanning microscope (FV1000, Olympus, Hamburg, Germany) using a 60× (NA 1.20) water-immersion objective with a custom built temperature chamber. R18 and BODIPY were excited with a 559 nm diode laser and the 488 nm line of an Ar-ion laser (Olympus, Hamburg, Germany), respectively. The emissions of R18 and BODIPY were recorded between 570 and 670 nm and between 500 and 530 nm, respectively.

**FTIR Spectroscopy.** For the infrared spectroscopic experiments, details on the preparation of large unilamellar vesicles in 20 mM Tris,

7 mM $MgCl_2$, pD 7.4, with included K-Ras4B ($c_{K\text{-}Ras}$ = 233 $\mu$M) are given in the Supporting Information. Measurements were performed at 25 °C with a Nicolet 5700 FTIR spectrometer equipped with a liquid nitrogen cooled MCT (HgCdTe) detector and a cell with $CaF_2$ windows separated by 50 $\mu$m mylar spacers. Typically, FTIR-spectra of 128 scans were taken with a resolution of 2 $cm^{-1}$ and correspondent processing was performed using GRAMS software (Thermo Electron). Details of the spectra correction and analysis are available in the Supporting Information.

## ■ ASSOCIATED CONTENT

**Supporting Information.** Complete refs 16 and 36. Details on materials and sample preparation. K-Ras4B protein synthesis: general aspects; cloning, expression, and purification of K-Ras4BΔ15-MESNA thioester, BODIPY labeling of the protein core thioester; nucleotide exchange on Ras proteins; ligation of K-Ras4B peptide with K-Ras4BΔ15-MESNA thioester. Details on the conduction of AFM, confocal laser scanning microscopy, FTIR, and IRRA spectroscopy experiments. Figures S1−S6 as described in the text. This material is available free of charge via the Internet at http://pubs.acs.org.

## ■ AUTHOR INFORMATION

**Corresponding Author**
roland.winter@tu-dortmund.de

## ■ ACKNOWLEDGMENT

This research was supported by the DFG (SFB 642 and SFB 740), the Max Planck Society (IMPRS), and the Leibniz-Graduate School "Molecular Biophysics". We are grateful to Christine Nowak for technical assistance.

## ■ REFERENCES

(1) Wittinghofer, A.; Waldmann, H. *Angew. Chem., Int. Ed.* **2000**, *39*, 4192–4214.
(2) Hancock, J. F. *Nat. Rev. Mol. Cell Biol.* **2003**, *4*, 373–384.
(3) Wittinghofer, A.; Pai, E. F. *Trends Biochem. Sci.* **1991**, *16*, 382–387.
(4) Bos, J. L. *Cancer Res.* **1989**, *49*, 4682–4689.
(5) Marshall, C. J. *Curr. Opin. Cell Biol.* **1996**, *8*, 197–204.
(6) Willumsen, B. M.; Christensen, A.; Hubbert, N. L.; Papageorge, A. G.; Lowy, D. R. *Nature* **1984**, *310*, 583–586.
(7) Hancock, J. F.; Paterson, H.; Marshall, C. J. *Cell* **1990**, *63*, 133–139.
(8) Yeung, T.; Gilbert, G. E.; Shi, J.; Silvius, J.; Kapus, A.; Grinstein, S. *Science* **2008**, *319*, 210–213.
(9) Okeley, N. M.; Gelb, M. H. *J. Biol. Chem.* **2004**, *279*, 21833–21840.
(10) Meder, D.; Simons, K. *Science* **2005**, *307*, 1731–1733.
(11) Jackson, J. H.; Li, J. W.; Buss, J. E.; Der, C. J.; Cochrane, C. G. *Proc. Natl. Acad. Sci. U.S.A.* **1994**, *91*, 12730–12734.
(12) Ghomashchi, F.; Zhang, X.; Liu, L.; Gelb, M. H. *Biochemistry* **1995**, *34*, 11910–11918.
(13) Silvius, J. R. *J. Membr. Biol.* **2002**, *190*, 83–92.
(14) Jansen, B.; Schlagbauer-Wadl, H.; Kahr, H.; Heere-Ress, E.; Mayer, B. X.; Eichler, H.; Pehamberger, H.; Gana-Weisz, M.; Ben-David, E.; Kloog, Y.; Wolff, K. *Proc. Natl. Acad. Sci. U.S.A.* **1999**, *96*, 14019–14024.
(15) Chen, Z.; Otto, J. C.; Bergo, M. O.; Young, S. G.; Casey, P. J. *J. Biol. Chem.* **2000**, *275*, 41251–41257.
(16) Bivona, T. G.;; et al. *Mol. Cell* **2006**, *21*, 481–493.
(17) Roy, M. O.; Leventis, R.; Silvius, J. R. *Biochemistry* **2000**, *39*, 8298–8307.
(18) Gomez, G. A.; Daniotti, J. L. *FEBS J.* **2007**, *274*, 2210–2228.
(19) Leventis, R.; Silvius, J. R. *Biochemistry* **1998**, *37*, 7640–7648.
(20) Plowman, S. J.; Muncke, C.; Parton, R. G.; Hancock, J. F. *Proc. Natl. Acad. Sci. U.S.A.* **2005**, *102*, 15500–15505.
(21) Prior, I. A.; Muncke, C.; Parton, R. G.; Hancock, J. F. *J. Cell Biol.* **2003**, *160*, 165–170.
(22) Plowman, S. J.; Ariotti, N.; Goodall, A.; Parton, R. G.; Hancock, J. F. *Mol. Cell. Biol.* **2008**, *28*, 4377–4385.
(23) Chen, Y.-X.; Koch, S.; Uhlenbrock, K.; Weise, K.; Das, D.; Gremer, L.; Brunsveld, L.; Wittinghofer, A.; Winter, R.; Triola, G.; Waldmann, H. *Angew. Chem., Int. Ed.* **2010**, *49*, 6090–6095.
(24) Weise, K.; Triola, G.; Brunsveld, L.; Waldmann, H.; Winter, R. *J. Am. Chem. Soc.* **2009**, *131*, 1557–1564.
(25) Bagatolli, L. A.; Gratton, E. *J. Fluoresc.* **2001**, *11*, 141–160.
(26) Weise, K.; Triola, G.; Janosch, S.; Waldmann, H.; Winter, R. *Biochim. Biophys. Acta* **2010**, *1798*, 1409–1417.
(27) Fujisawa, T.; Uruga, T.; Yamaizumi, Z.; Inoko, Y.; Nishimura, S.; Ueki, T. *J. Biochem.* **1994**, *115*, 875–880.
(28) Vogel, A.; Reuther, G.; Weise, K.; Triola, G.; Nikolaus, J.; Tan, K.-T.; Nowak, C.; Herrmann, A.; Waldmann, H.; Winter, R.; Huster, D. *Angew. Chem., Int. Ed.* **2009**, *48*, 8784–8787.
(29) Tamm, L. K.; Tatulian, S. A. *Q. Rev. Biophys.* **1997**, *304*, 365–429.
(30) Milburn, M. V.; Tong, L.; deVos, A. M.; Brünger, A.; Yamaizumi, Z.; Nishimura, S.; Kim, S. H. *Science* **1990**, *247*, 939–945.
(31) Meister, A.; Nicolini, C.; Waldmann, H.; Kuhlmann, J.; Kerth, A.; Winter, R.; Blume, A. *Biophys. J.* **2006**, *91*, 1388–1401.
(32) Scheiffele, P.; Rietveld, A.; Wilk, T.; Simons, K. *J. Biol. Chem.* **1999**, *274*, 2038–2044.
(33) Nicolini, C.; Baranski, J.; Schlummer, S.; Palomo, J.; Burgues, M. L.; Kahms, M.; Kuhlmann, J.; Sanchez, S.; Gratton, E.; Waldmann, H.; Winter, R. *J. Am. Chem. Soc.* **2006**, *128*, 192–201.
(34) Rocks, O.; Peyker, A.; Kahms, M.; Verveer, P. J.; Koerner, C.; Lumbierres, M.; Kuhlmann, J.; Waldmann, H.; Wittinghofer, A.; Bastiaens, P. I. *Science* **2005**, *307*, 1746–1752.
(35) Rocks, O.; Gerauer, M.; Vartak, N.; Koch, S.; Huang, Z. P.; Pechlivanis, M.; Kuhlmann, J.; Brunsveld, L.; Chandra, A.; Ellinger, B.; Waldmann, H.; Bastiaens, P. I. *Cell* **2010**, *141*, 458–471.
(36) Dekker, F. J.;; et al. *Nat. Chem. Biol.* **2010**, *6*, 449–456.
(37) Bunge, A.; Kurz, A.; Windeck, A.-K.; Korte, T.; Flasche, W.; Liebscher, J.; Herrmann, A.; Huster, D. *Langmuir* **2007**, *23*, 4455–4464.
(38) McLaughlin, S.; Murray, D. *Nature* **2005**, *438*, 605–611.
(39) Golebiewska, U.; Gambhir, A.; Hangyás-Mihályné, G.; Zaitseva, I.; Rädler, J.; McLaughlin, S. *Biophys. J.* **2006**, *91*, 588–99.
(40) Heo, W. D.; Inoue, T.; Park, W. S.; Kim, M. L.; Park, B. O.; Wandless, T. J.; Meyer, T. *Science* **2006**, *314*, 1458–1461.
(41) Ben-Tal, N.; Honig, B.; Peitzsch, R. M.; Denisov, G.; McLaughlin, S. *Biophys. J.* **1996**, *71*, 561–575.
(42) Idema, T.; Semrau, S.; Storm, C.; Schmidt, T. *Phys. Rev. Lett.* **2010**, *104*, 198102.
(43) Tian, T.; Harding, A.; Inder, K.; Plowman, S.; Parton, R. G.; Hancock, J. F. *Nat. Cell Biol.* **2007**, *9*, 905–914.
(44) Lowy, D. R.; Willumsen, B. M. *Annu. Rev. Biochem.* **1993**, *62*, 851–891.
(45) Abankwa, D.; Gorfe, A. A.; Inder, K.; Hancock, J. F. *Proc. Natl. Acad. Sci. U.S.A.* **2010**, *107*, 1130–1135.
(46) Angelova, M. I.; Soleau, S.; Meleard, P.; Faucon, F.; Bothorel, P. *Prog. Colloid Polym. Sci.* **1992**, *89*, 127–131.
(47) Janosch, S.; Nicolini, C.; Ludolph, B.; Peters, C.; Völkert, M.; Hazlet, T. L.; Gratton, E.; Waldmann, H.; Winter, R. *J. Am. Chem. Soc.* **2004**, *126*, 7496–7503.
(48) Johnson, S. A.; Stinson, B. M.; Go, M. S.; Carmona, L. M.; Reminick, J. I.; Fang, X.; Baumgart, T. *Biochim. Biophys. Acta* **2010**, *1798*, 1427–1435.
(49) Bligh, E. G.; Dyer, W. J. *Can. J. Biochem. Physiol.* **1959**, *37*, 911–917.